CrystEngComm

Accepted Manuscript

ROYAL SOCIETY OF CHEMISTRY

www.rsc.org/crystengcomm

Superlattice-like $SnSb_4$/Ge thin films for ultra-high speed phase change memory applications

Zifang He,[a] Pengzhi Wu,[b] Ruirui Liu,[a] Jiwei Zhai,[a, 1)] Tianshu Lai,[b, 2)] Sannian Song,[c] Zhitang Song[c]

[a]Key Laboratory of Advanced Civil Engineering Materials of Ministry of Education, Functional Materials Research Laboratory, School of Materials Science & Engineering, Tongji University, Shanghai 201804, China

[b]State Key Laboratory of Optoelectronic Materials and Technology, Department of Physics, Sun Yat-Sen University, Guangzhou 510275, China

[c]State Key Laboratory of Functional Materials for Informatics, Shanghai Institute of Micro-system and Information Technology, Chinese Academy of Sciences, Shanghai 200050, China

Abstract

Superlattice-like (SLL) $SnSb_4$/Ge thin films were studied by the thermal, electrical and optical methods. It was found that $SnSb_4$ (SS) films composited with Ge by superlattice-like configuration showed better thermal stability. With Ge composited, the temperature of 10-year data retention increased from 54 °C to 139 °C. In the electrical studies, reversible transition of the phase change memory cell based on the $[SS(8\ nm)/Ge(4\ nm)]_4$ could be achieved by using an electrical pulse of as short as 500 ns. Moreover, ultrafast crystallization (~6.54 ns at a energy density of ~4.47 mJ/cm^2) in the $[SS(8\ nm)/Ge(4\ nm)]_4$ film was confirmed, which was essential to achieve rapid data recording in phase change memory.

Introduction

Flash memory is restricted by its physical limitation beyond the 22 nm node technology although it has been successfully used as nonvolatile semiconductor memory [1]. Therefore, phase change memory (PCM) has recently emerged as a potential candidate for next-generation nonvolatile memory applications [2]. The phase transformation of PCM is invoked by Joule heating. The data access relies on the fast reversible switching between the amorphous state (high resistivity) and the

Corresponding author. E-mail address: 1) apzhai@tongji.edu.cn, 2) stslts@mail.sysu.edu.cn.

crystallization state (low resistivity).

$Ge_2Sb_2Te_5$ (GST) has been widely studied in recent years as it exhibits relatively good performances [3, 4]. However, the commercial using GST is encountering a key issue - a relatively low temperature of 10-year data retention (89 °C) [5], which results in poor thermal stability making it invalid for the PCM applications such as automotive electronics (about 125 °C). Besides, the switching speed, which is limited by its nucleation-dominated crystallization mechanism, is not comparable with dynamic random access memory (DRAM) (10 ns) [6, 7]. Recently, intensive methods such as doping and compositing have been performed to improve the performances of phase change materials (PCMs). Sn-doped GST materials exhibited higher switching speed [8]. Nitrogen implantation in GST film can raise its thermal stability [9]. In addition, superlattice-like (SLL) thin films exhibit many attractive electrical, optical and thermal properties which are associated with the periodic nature of SLL and the repeat thickness in the structure, such as quantum size effects [10]. Superlattice-like (SLL) $SiO_2/Sb_{80}Te_{20}$ films have been confirmed to have rapid crystallization speed [11]. SLL Ge/Sb_2Te_3 films showed better thermal stability [12]. The PCMs with SLL structure have been confirmed to have ultra-low thermal conductivity and good thermal confinement properties due to the phonon scattering effects at the interfaces [13, 14].

In this work, SLL $SnSb_4/Ge$ thin films are prepared by $SnSb_4$ and Ge. $SnSb_4$ has fast switching speed but poor thermal stability [15]. By incorporating with Ge, the fast switching speed is hold and thermal stability is improved.

Experimental details

SLL $SnSb_4/Ge$ thin films with different thickness ratios were deposited on SiO_2/Si (100) wafers by using a radio-frequency (RF) magnetron sputtering system at room temperature with $SnSb_4$ and Ge targets, respectively. The total thickness of all thin films was about 50 nm. The thickness of each layer was controlled by deposition time. The background pressure was under 1×10^{-4} Pa. All deposition processes were carried out in Ar atmosphere at a pressure of 0.2 Pa, with a flow of 30 sccm and an RF power of 20 W. An automatic rotation of 20 rpm for the substrate was used to guarantee a uniform deposition.

Resistance as a function of the temperature (*R*–*T*) was measured in situ in Ar atmosphere by using a two-point-probe set-up to obtain the crystallization temperature. The thin films were kept at different temperatures for isothermal *R*–*T* measurements to estimate the data retention time and the activation energy (E_a) for crystallization by using the Arrhenius equation. The crystalline phases of the films were analyzed by X-ray diffraction (XRD, Rigaku D/MAX 2550 V) with Cu Kα radiation in the 2θ degree range from 20° to 60°, with a scanning step of 1°/min. Cross-sectional morphology and electronic diffraction patterns of the thin films were characterized by using an FEI CM200 FEG analytical transmission electron microscope (TEM) with an operating voltage of 160 kV. A picosecond laser pump–probe system was used for real-time reflectivity measurements. The light source used for irradiating the samples was a frequency-doubled model-locked neodymium yttrium aluminum garnet laser operating at 532 nm wavelength with a pulse duration of 30 ps. PCM cells based on the SSL thin film $[SS(8\ nm)/Ge(4\ nm)]_4$ were fabricated according to the CMOS technology. *I-V* and *R*–*V* curves were measured with a Keithley-2400 digital source meter, and an Agilent-81104A pulse generator was used to provide the voltage pulse.

Results and discussion

Fig. 1(a) shows the resistance (*R*) as a function of temperature (*R*-*T*) for SLL $SnSb_4$/Ge thin films at a heating rate of 10 °C/min. The amorphous $SnSb_4$/Ge films are characterized by a relatively high resistance at room temperature, which is stable with the increasing temperature until an abrupt drop at the crystallization temperature (T_c). With increasing thickness of Ge in SLL $SnSb_4$/Ge thin films, T_c value of the samples goes up from 160 °C to 202 °C , all of which are higher than that of GST films (150 °C) [16], which is attributed to the better thermal stability of amorphous Ge [17]. The change in the sheet resistance across the crystallization temperature in

SLL $SnSb_4$/Ge thin films is even sharper than that of GST when the films transform from an amorphous to a crystalline state, indicating that the SLL $SnSb_4$/Ge films could have a much faster crystallization speed than the GST film. In addition, the amorphous resistance of SLL $SnSb_4$/Ge films also increases with increasing thickness of Ge, which is believed to be associated with the high resistance of Ge ($\sim10^6$ Ω) and the interfacial effect [18].

Data retention is another important parameter for PCM applications, generally determined by thermal stability of the amorphous films. It is characterized by failure time which is defined as the time required for the Rs falling to half of its initial value at a specific temperature [19]. Fig. 1(b) is the best fit of failure time vs. reciprocal temperature ($1/k_BT$) using the Arrhenius equation: $t = \tau \exp(E_a/ k_BT)$, where t is the time to failure, τ is a proportional time constant, E_a is the crystalline activation energy and k_B is Boltzmann's constant [20]. As shown in the figure, E_a and 10 year data retention of SLL $SnSb_4$/Ge films increase obviously with increasing Ge thickness ratio, and both of them among all $SnSb_4$/Ge films are higher than that of GST film (85 °C, 2.24 eV) [16]. It means SLL $SnSb_4$/Ge films have better thermal stability than GST.

Fig. 2 shows the XRD patterns of homogeneous $SnSb_4$ film and SSL [$SnSb_4$(8 nm)/Ge(4 nm)]$_4$ films in as-deposited state and after annealing at 250°C for 10 minutes. It can be seen from Fig. 2(a), no diffraction peaks appear in as-deposited state. After annealing, $SnSb_4$ film has been crystallized into SnSb and Sb phases. Fig. 2(b) depicts that the tiny diffraction peak (012) Sb appears in as-deposited state, which is resulted from the crystallization of Sb ingredient with low crystallization temperature during deposition. In addition, compared with homogeneous $SnSb_4$ film, there are only Sb peaks in the pattern of [$SnSb_4$(8 nm)/Ge(4 nm)]$_4$ film after annealing at 250°C. It should be noticed that the disappearance of SnSb phase demonstrates that the insertion of Ge layers restrains the crystallization of $SnSb_4$, which not only eases the concern of phase separation but improves the thermal stability for PCM applications. The presence of Ge layer makes it impossible for small grains to coalesce and grow in vertical direction. Plenty of Ge-Sn bond and Ge-Sb bond may exist nearby the interface of Ge layers and $SnSb_4$ layers which could block the growth of grains [21].

Crystallization is usually accompanied with the change of resistivity as well as optical reflectivity. Hence, two consecutive picosecond laser pulses with different laser fluences were used to evaluate the phase-change speed. Fig. 3 shows the normalized reflectivity evolution of the SLL $[SS(8\ nm)/Ge(4\ nm)]_4$ thin film. As shown in Fig. 3(a), the initial low reflectivity increases rapidly to a relatively higher level with an irradiation fluence of 4.47 mJ/cm^2, corresponding to the transition from amorphous to crystalline state. With a higher laser pulse fluence of 7.11 mJ/cm^2, the amorphization of SLL $[SS(8\ nm)/Ge(4\ nm)]_4$ film is achieved with the drop of optical reflectivity (Fig. 3(b)). Based on these results, it is shown that the reversible phase change can be realized by employing laser pulses with different energy densities. Above all, the SLL $[SS(8\ nm)/Ge(4\ nm)]_4$ thin film displays a ultrafast crystallization speed (6.54 ns), which is about one third that of GST (17.7 ns). And the amorphization process of the film also has a faster phase-change speed (4.21 ns) than GST (16.5 ns). It is reported that the excessive Sb atoms in the Sb-rich phase-change materials would form a large number of Sb nucleus. During crystallization, the dispersed Sb nucleus can act as heterogeneous nucleating centers, which facilitated crystallization [22]. And the growth-dominated crystallization mechanism of $SnSb_4$ is also related to its ultrafast phase change speed [23].

Cross-sectional TEM images of the $[SS(8\ nm)/Ge(4\ nm)]_4$ film are presented in Fig. 4 (a) and (b) along with its corresponding selected area electron diffraction (SAED) patterns in the inset. For as-deposited film (Fig. 4 (a)), the interfaces between the $SnSb_4$ and Ge layers are very clear and the diffusive ring pattern in the inset reveals the amorphous structures. After annealing at 300 °C for 10 min (Fig. 4 (b)), the interfaces are less sharp, but the SLL structure can still be observed, and no obvious diffusion is emerged between the two layers. The SAED pattern in the inset shows that the film has been well crystallized. By carefully indexing, the thermally induced crystals of [SS(8 nm)/Ge(4 nm)]$_4$ film can be assigned to an A7-type structure similar to Sb with rhomb-centered configuration [24] which is agreed with the results of XRD patterns. High-resolution transmission electron microscopy (HRTEM) images as shown in Fig. 4(c) and 4(d) reveal that the measured interplanar distances match with those in crystalline Sb phase very well. The TEM observations further validate the good thermal stability of SLL structure, which has a positive effects on operation reliability of the PCM.

The T-shaped PCM cells based on SLL [SS(8 nm)/Ge(4 nm)]$_4$ thin films were prepared by using the 0.18 μm CMOS technology. The inset in Fig. 5 shows the schematic diagram of the cross-sectional PCM cell configuration. Tungsten was used as a heating electrode 260 nm in diameter. The [SS(8 nm)/Ge(4 nm)]$_4$ thin film, TiN contact layer and Al top electrode were deposited by sputtering method with the thickness 50, 20 and 200 nm, respectively. Fig. 5(a) shows the I-V curve of the film, exhibited a threshold switching phenomenon from a high-resistivity state to a low-resistivity state beyond the threshold voltage (V_{th}). The V_{th} of [SS(8 nm)/Ge(4 nm)]$_4$ thin film is about 1.35 V, which is much lower than that of $Ge_2Sb_2Te_5$ film (2.35 V). Fig. 5(b) shows the resistance dependence of the pulse voltage with different pulse widths. As the pulse widths decrease from 1000 to 500 ns, the reset voltage increases from 2.6 to 2.9 V. Obviously, the reset voltage of the cells based on [SS(8 nm)/Ge(4 nm)]$_4$ thin film with the pulse width 500 ns is lower than that of GST (3.5V). In the resistance switching of PCM cells, the “reset” operation needs much higher power than the “set” operation. Therefore, we pay more attention to the reset power. According to the formula for the power $E_{RESET} = V_{RESET}{}^2 / R_{SET} \times t_{RESET}$, the cell based on [SS(8 nm)/Ge(4 nm)]$_4$ thin film (2.9V, 10^4 Ω, 500ns) shows a lower reset power consumption than that of GST (3.5V, 10^4 Ω, 500ns).

Conclusions

In summary, SLL $SnSb_4$/Ge thin films have been studied for ultrafast speed PCM application. The optimized configuration SLL [SS(8 nm)/Ge(4 nm)]$_4$ thin film shows better thermal stability, lower power consumption and ultrafast phase transition. E_a and 10 year data retention of SLL [SS(8 nm)/Ge(4 nm)]$_4$ film (2.89 eV, 119 °C) are both larger than those of GST film (2.24 eV, 85 °C). The current–voltage and resistance–voltage measurements of PCM cells based on [SS(8 nm)/Ge(4 nm)]$_4$ thin films exhibited a lower threshold voltage of set (2.48V) and reset (2.68V) operations compared with GST, indicating the lower power consumption. Meanwhile, the phase-change times of [SS(8 nm)/Ge(4 nm)]$_4$ are 6.54 and 4.21 ns for crystallization and amorphization processes, respectively. An ultrafast switching speed is achieved due to the Sb-rich chemical composition and growth-dominated crystallization mechanism of the phase change materials.

Acknowledgements

The authors would like to acknowledge financial support from the Natural Science Foundation of China under Grant No. 61474083.

Notes and references

1 G.. J. Meijer, Science, 2008, **319**, 1625.

2 H. Yang, C. T. Chong, R. Zhao, H. K. Lee , J . Li, K. G. Lim, Appl. Phys. Lett., 2009, **94**, 203110.

3 T. Morikawa, K. Kurotsuchi, Y. Fujisaki, Y. Matsui, N. Takaura. Japanese Journal of Applied Physics., 2012, **51**, 031201.

4 J. Tominaga, R. E. Simpson, P .Fons, A. V. Kolobov, Appl. Phys. Lett., 2011, **99**, 152105.

5 W. Zhou, L. C. Wu, X. Zhou, F. Rao, Z. T. Song, D. Yao, Appl. Phys. Lett., 2014, **105**, 243113.

6 C. Peng, L. C. Wu, F. Rao, Z. T. Song, X. Zhou, M. Zhu, Scri. Mater., 2011, **65**, 327.

7 X. Zhou, L. C. Wu, Z. T. Song, F. Rao, B. Liu, D. Yao, Appl. Phys. A., 2010, **103**, 1077.

8 M. L. Lee, K.T. Yong, C. L. Gan, L. H. Ting, Daud. S. B. Muhamad, L. P. Shi. J. Phys. D., 2008, **41**, 215402.

9 L. Cheng, L. Wu, Z. T. Song, F. Rao, C. Peng, D. Yao, J. Appl. Phys., 2013, **113**, 044514.

10 T. C. Chong, L. P. Shi, X. Q. Wei, R. Zhao, H. K. Lee, P. Yang, Physl. Revi. Lett., 2008, **100**.

11 C. Z. Wang, J. W. Zhai, Z. T. Song, F. Shang, X. Yao. Appl. Phys. A ., 2010, **103**, 193.

12 C. Z. Wang, J. W. Zhai, Z. T. Song, F. Shang, X. Yao. Appl. Surf. Sci., 2010, **257**, 949.

13 D. Loke, L. Shi, W. Wang, R. Zhao, H. Yang, L. T. Ng, Nanotechnology, 2011, **22**, 254019.

14 S. Soeya, T. Shintani, T. Odaka, R. Kondou, J. Tominaga, Appl. Phys. Lett., 2013, **103**, 053103.

15 Y. F. Hu, J. W. Zhai, H. R. Zeng, S. N. Song, Z. T. Song, J. Appl. Phys., 2015, **117**, 175704.

16 I. Friedrich, V. Weidenhof, W. Njoroge, P. Franz, M. Wuttig, J. Appl. Phys., 2000, **87**, 4130.

17 Y. F. Hu, X. Y. Feng, J. W. Zhai, T. Wen, T. S. Lai, S. N. Song, Z. T. Song, Scri. Mater., 2014, **93**, 4-7.

18 S. Raoux, B. Muñoz, H. Y. Cheng, J. L. Jordan-Sweet, Appl. Phys. Lett., 2009, **95**, 143118.

19 K. F. Kao, C. C. Chang, F. T. Chen, M. J. Tsai, T. S. Chin. Scri. Mater., 2010, **63**, 855.

20 M. Wuttig, C. Steimer. Appl. Phys. A 2007, **87**, 411.

21 M. C. Sun, Y. F. Hu, B. Shen, J. W. Zhai, S. N. Song, Z. T. Song, Integrated Ferroelectrics 2012, **140**, 1.

22 Y. F. Hu, S. M. Li, T .S. Lai, S. N. Song, Z. T. Song, J. W. Zhai, Scri. Mater., 2013, **69**, 61.

23 F. Rao, Z. T. Song, K. Ren, X. Li, L. C. Wu, W. Xi, Appl. Phys. Lett. 2009, **95**, 032105.

24 X. L. Zhou, L. C. Wu, Z. T. Song, F. Rao, K. Ren, C. Peng, Appl. Phys. Lett., 2013, **103**, 072114.

Figure captions:

Fig. 1 (a) Resistance as a function of temperature for the SLL $SnSb_4$/Ge thin films with different thickness ratio and $SnSb_4$ monolayer thin films at a heating rate of 10 °C/min; (b) Plots of failure time as a function of reciprocal temperature for the SLL $SnSb_4$/Ge thin films.

Fig. 2. XRD patterns of (a) $SnSb_4$, (b) $[SS(8\ nm)/Ge(4\ nm)]_4$ at as-deposited state and annealed at 250 ^{o}C for 10 min, respectively.

Fig. 3. Reversible reflectivity evolution of the SLL $[SS(8\ nm)/Ge(4\ nm)]_4$ thin film induced by consecutive picosecond laser pulses with different fluencies: (a) crystallization process, (b) amorphization process.

Fig. 4. The cross-sectional TEM images and SAED patterns of SLL $[SS(8\ nm)/Ge(4\ nm)]_4$ thin films: (a) as-deposited, (b) annealed at 300 ^{o}C for 10 min, (c) and (d) the HRTEM images of the annealed film.

Fig. 5. (a) I–V and (b) R–V curves of the PCRAM cells based on the SLL $[SS(8\ nm)/Ge(4\ nm)]_4$ thin film.

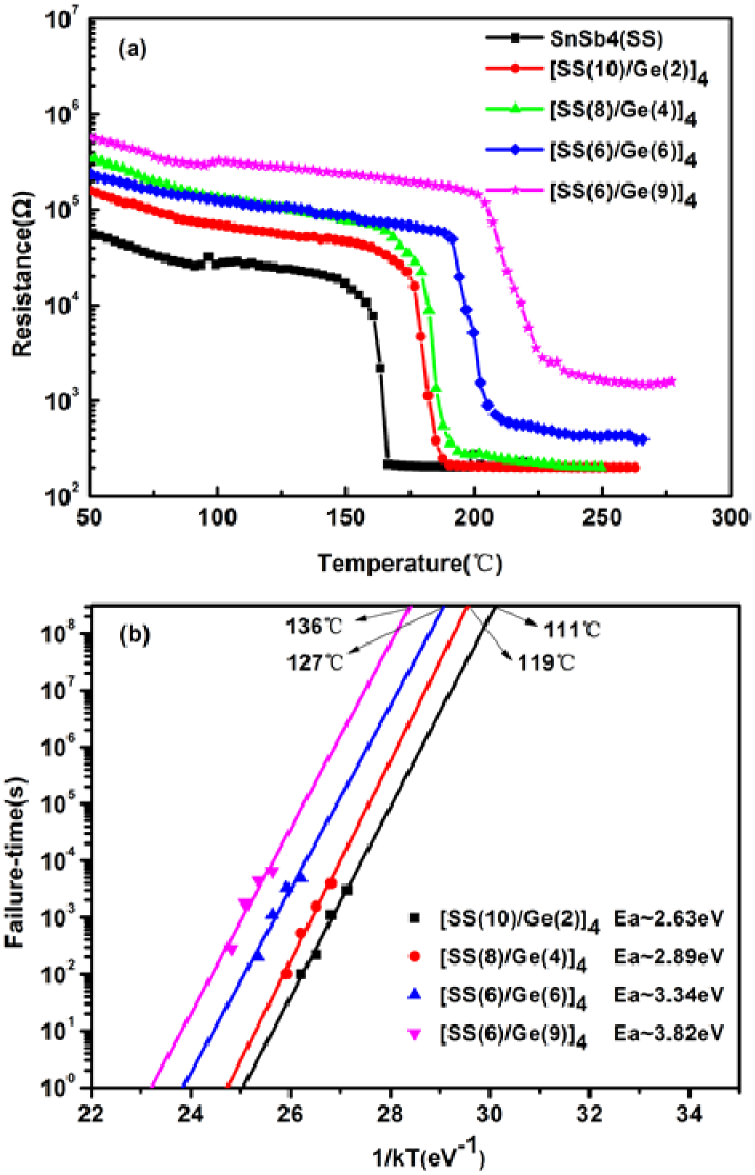
(a)
SnSb4(SS)
[SS(10)/Ge(2)]4
[SS(8)/Ge(4)]4
[SS(6)/Ge(6)]4
[SS(6)/Ge(9)]4
Resistance(Ω)
10^7
10^6
10^5
10^4
10^3
10^2
50
100
150
200
250
300
Temperature(℃)
(b)
136℃
127℃
111℃
119℃
[SS(10)/Ge(2)]4 Ea~2.63eV
[SS(8)/Ge(4)]4 Ea~2.89eV
[SS(6)/Ge(6)]4 Ea~3.34eV
[SS(6)/Ge(9)]4 Ea~3.82eV
Failure-time(s)
10^8
10^7
10^6
10^5
10^4
10^3
10^2
10^1
10^0
22
24
26
28
30
32
34
1/kT(eV^{-1})

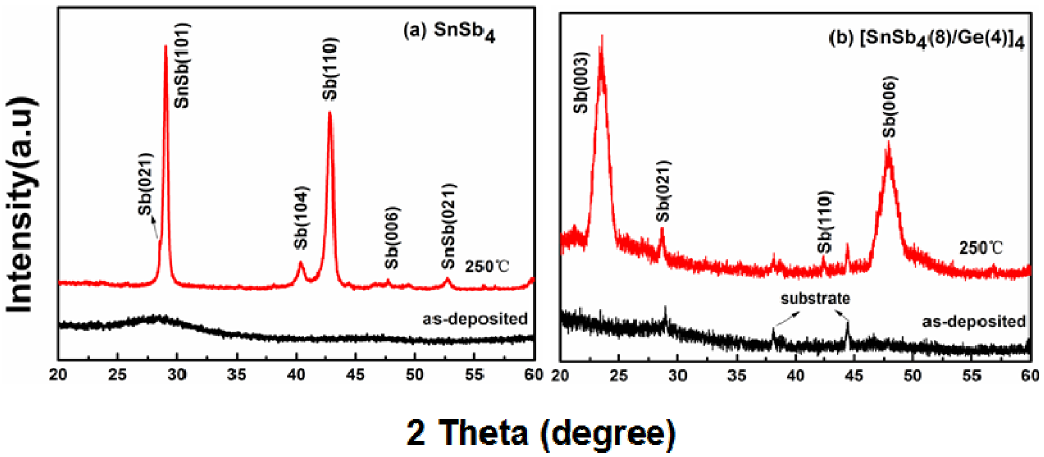
Intensity(a.u)
(a) SnSb$_4$
Sb(021)
SnSb(101)
Sb(104)
Sb(110)
Sb(006)
SnSb(021)
250℃
as-deposited
20
25
30
35
40
45
50
55
60
(b) [SnSb$_4$(8)/Ge(4)]$_4$
Sb(003)
Sb(021)
Sb(110)
Sb(006)
250℃
substrate
as-deposited
20
25
30
35
40
45
50
55
60
2 Theta (degree)

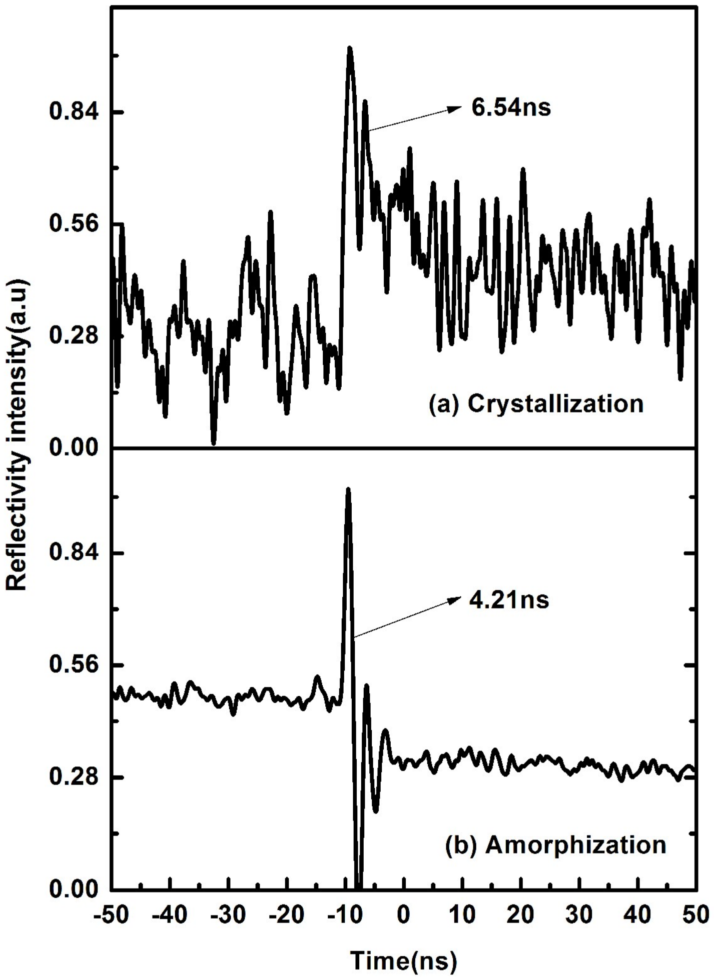
Reflectivity intensity(a.u)
0.84
0.56
0.28
0.00
6.54ns
(a) Crystallization
4.21ns
(b) Amorphization
-50
-40
-30
-20
-10
0
10
20
30
40
50
Time(ns)

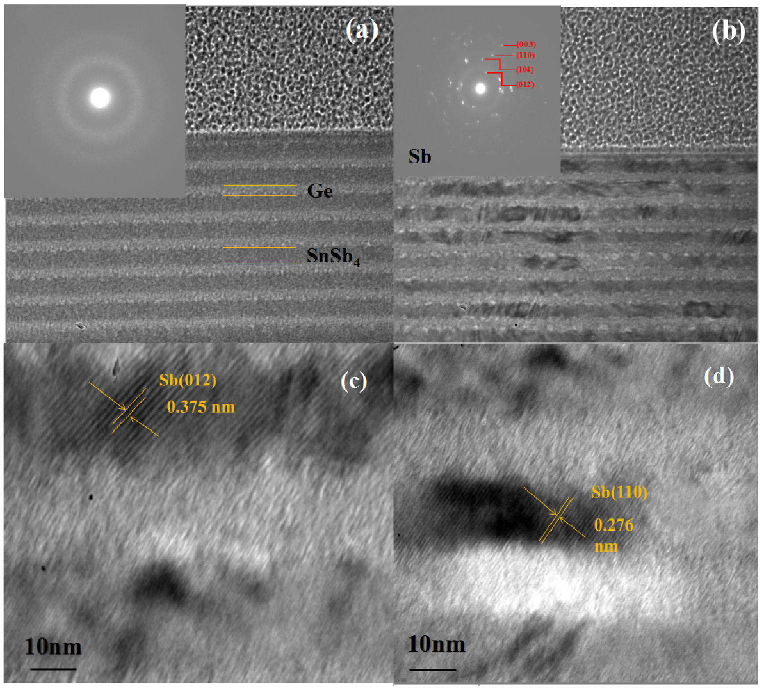
(a)
Ge
SnSb4
(b)
(003)
(110)
(104)
(012)
Sb
(c)
Sb(012)
0.375 nm
10nm
(d)
Sb(110)
0.276 nm
10nm

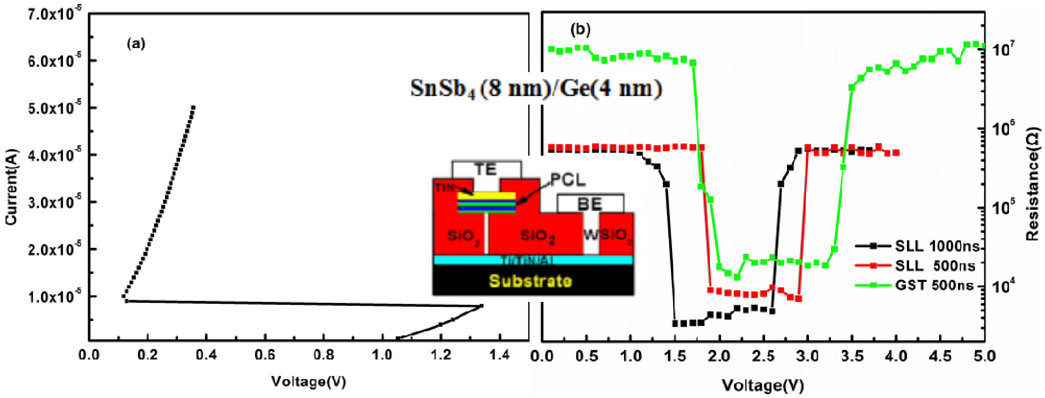
(a)
Current(A)
7.0x10^{-5}
6.0x10^{-5}
5.0x10^{-5}
4.0x10^{-5}
3.0x10^{-5}
2.0x10^{-5}
1.0x10^{-5}
0.0
0.2
0.4
0.6
0.8
1.0
1.2
1.4
Voltage(V)
SnSb$_4$(8 nm)/Ge(4 nm)
TE
PCL
TiN
BE
SiO$_2$
SiO$_2$
W
SiO$_2$
Ti/TiN/Al
Substrate
(b)
Resistance(Ω)
10^7
10^6
10^5
10^4
0.0
0.5
1.0
1.5
2.0
2.5
3.0
3.5
4.0
4.5
5.0
Voltage(V)
SLL 1000ns
SLL 500ns
GST 500ns